Reaction channel contributions to the triton + ^{208}Pb optical potential

N. Keeley*
National Centre for Nuclear Research, ul. Andrzeja Sołtana 7, 05-400 Otwock, Poland

R. S. Mackintosh†
School of Physical Sciences, The Open University, Milton Keynes MK7 6AA, United Kingdom

(Received 8 December 2022; accepted 23 February 2023; published 3 March 2023)

Background: Well-established coupled channel and coupled reaction channel (CRC) processes make contributions to elastic scattering that are not included in standard folding models of the optical model potential (OMP). Such contributions have been established for ^{3}He interacting with ^{208}Pb but the corresponding contributions for ^{3}H are expected to be different, particularly for pickup coupling.
Purpose: To establish and characterize the contribution to the interaction potential between ^{3}H and ^{208}Pb that is generated by coupling to proton pickup (outgoing ^{4}He) channels; also to study the contribution of collective states and identify effects of dynamical nonlocality due to these couplings.
Methods: CRC calculations, including coupling to collective states, will provide the elastic channel S-matrix S_{lj} resulting from the included processes. Inversion of S_{lj} will produce the local potential that yields, in a single channel calculation, the elastic scattering observables from the coupled channel calculation. Subtracting the bare potential from the inverted CRC potential yields a local and l-independent representation of the dynamical polarization potential (DPP). From the DPPs due to a range of combinations of channel couplings, the influence of dynamically generated nonlocality can be identified.
Results: Coupling to ^{4}He channels makes a smaller contribution to the ^{3}H interaction than it does for incident ^{3}He. On the other hand coupling to inelastic channels makes a greater contribution than it does for ^{3}He. The nonadditivity of the DPPs implies their dynamical nonlocality.
Conclusions: The DPPs established here challenge the notion that folding models, in particular local density models, provide a satisfactory description of elastic scattering of ^{3}H from nuclei. Coupling to proton pickup channels induces dynamical nonlocality in the ^{3}H OMP with implications for direct reactions involving ^{3}H. Departures from a smooth radial form for the ^{3}H OMP should be apparent in high quality fits to suitable elastic scattering data. Future theories of the interaction of ^{3}H with nuclei should include some representation of outgoing ^{4}He.

DOI: 10.1103/PhysRevC.107.034602

I. INTRODUCTION

Recent advances in microscopic calculations of the optical model potential (OMP) have seen an increasingly sophisticated array of techniques brought to bear on this complex problem for both nucleon scattering, e.g., Refs. [1–4] and references therein, and light composite projectiles, e.g., Ref. [5] and references therein. Although these calculations frequently incorporate such refinements as many-body contributions to the nucleon-nucleon force and explicit treatment of exchange nonlocality they usually neglect contributions from collective excitations and rearrangement (transfer) processes. In a series of studies over the past decade we have demonstrated that these processes can make a significant contribution to the OMP for both nucleons and composite projectiles, in particular pickup reactions on closed-shell targets. Any complete approach to a calculation of the OMP should therefore explicitly include such processes. This has been done by applying a well-established procedure for S_{lj}-to-potential inversion of the elastic channel S matrix, S_{lj}, resulting from specific reaction and/or inelastic couplings in a coupled channel (CC) calculation, see, e.g., Ref. [6], (CC refers throughout to both collective and reaction channel coupling). The CC calculations take structure input from the literature [spectroscopic factors, $B(E\lambda)$ values. etc.] to fix the coupling strengths, and the parameters of the diagonal (or "bare") optical potential in the entrance channel are adjusted so that the full CC result gives a good description of a chosen elastic scattering data set, including polarization observables where this is appropriate and suitable data are available.

Two previous works [7,8] studied the contributions of collective excitations and nucleon pickup to the OMPs for ^{3}He and ^{3}H on ^{16}O and ^{40}Ca while Ref. [7] examined the influence of the same couplings for ^{3}He on ^{208}Pb. The formal contribution of collective and reaction channel processes to OMPs, the dynamical polarization potential (DPP) is both

*nicholas.keeley@ncbj.gov.pl
†raymond.mackintosh@open.ac.uk

nonlocal and l dependent [9–11]. This dynamical nonlocality [12] is distinct from nonlocality due to exchange processes. However, the contribution of reaction channel and collective coupling can be represented by a local and l-independent addition to the phenomenological OMP that yields the same S matrix, S_{lj}, providing a link to standard phenomenology and local-density folding models. It is this local, l-independent S-matrix-equivalent DPP which is the result of the inversion procedure.

It was shown that pickup and inelastic couplings make significant contributions to the OMP for ^{3}He and ^{3}H scattering from ^{16}O and ^{40}Ca [7,8], with a relatively smaller contribution for ^{3}He on ^{208}Pb [7]. A significant finding was dynamical nonlocality of the DPPs, the evidence being the nonadditivity of the local equivalent DPPs for different couplings. The formal, nonlocal (and l-dependent) DPP generated by coupling to a number of nonmutually coupled channels is equal to the sum of the individual nonlocal DPPs generated by coupling to each of the channels separately. This is not true of their local equivalents: the sum of the individual local equivalent DPPs is not the local equivalent DPP for the calculation where all the couplings are included simultaneously. The degree of nonadditivity is a measure of the importance of the nonlocality generated by the couplings. See Refs. [6] and [12] for further discussion of this point. All the systems studied here revealed substantial dynamical nonlocality of the induced DPPs.

Comparison of the DPPs for the two mass-three projectiles was previously limited to the ^{16}O and ^{40}Ca cases for two reasons: (1) the relatively low atomic number of these targets limits the influence of the different Coulomb barriers for ^{3}He and ^{3}H, and (2) structure effects on the neutron pickup (for ^{3}He) and proton pickup (for ^{3}H) should be largely due to differences in reaction Q values since they involve the same shell model orbitals (hence the same angular momentum transfers and to a large extent similar spectroscopic factors) due to the self-conjugate nature of the targets. It was found [8] that while the DPPs for the two projectiles were broadly similar, notably in an apparent trend for the magnitudes to decrease with increasing Q value, the pickup DPPs for ^{3}He were systematically larger.

In this work we extend this comparison to include both ^{3}H and ^{3}He on ^{208}Pb by determining the relevant local equivalent DPPs for $^3\mathrm{H} + {}^{208}$Pb. More important differences between the DPPs for ^{3}H and ^{3}He projectiles incident on this heavy target might be expected, in part because of the much larger Coulomb barrier difference. Also significant for pickup are the different orbitals and thus angular momentum transfers and spectroscopic factors. In contrast with the cases involving lighter nuclei, ^{16}O or ^{40}Ca, the difference in pickup Q values for ^{3}H and ^{3}He is significantly smaller for a ^{208}Pb target: +11.8 MeV for (^{3}H, ^{4}He) versus +13.2 MeV for (^{3}He, ^{4}He) compared with +11.5 MeV versus +4.9 MeV for ^{40}Ca and +7.7 MeV versus +4.9 MeV for ^{16}O.

II. PICKUP AND INELASTIC CONTRIBUTIONS TO THE OMP

We follow the same procedure for determining the DPPs as in Refs. [7] and [8], exploiting S_{lj}-to-potential inversion for CC calculations involving specific reaction and/or inelastic couplings. The difference between the resulting potential and the so-called bare potential, the entrance channel optical potential of the CC calculation, is a local equivalent of the nonlocal and l-dependent formal DPP generated by the couplings. Thus the S matrix, and therefore the elastic scattering observables, will be identical in two cases: (1) when the coupling is turned on with the bare potential in the elastic channel, and (2) when the DPP is added to the bare potential without channel coupling. It has been found that DPPs determined in this way are not strongly dependent on the particular bare potential employed. In what follows "DPP" will refer to the local equivalent of the formal DPP unless otherwise stated. All reaction calculations were carried out with the FRESCO code [13].

The $^3\mathrm{H} + {}^{208}$Pb CC calculations were as similar as possible to the $^3\mathrm{He} + {}^{208}$Pb calculations of Ref. [8] and were carried out for an incident ^{3}H energy of 33 MeV. Pickup coupling to the following single proton hole states of ^{207}Tl was included: the 0.00-MeV $1/2^+$ ($l = 0$), the 0.35-MeV $3/2^+$ ($l = 2$), the 1.35-MeV $11/2^-$ ($l = 5$), the 1.67-MeV $5/2^+$ ($l = 2$), and the 3.47-MeV $7/2^+$ ($l = 4$). Inelastic coupling to the 2.615-MeV 3^- and 4.085-MeV 2^+ collective states of ^{208}Pb was also included.

The $\langle {}^4\mathrm{He} \mid {}^3\mathrm{H} + p \rangle$ overlap was taken from Brida *et al.* [14], as in the CC calculations of Ref. [8], and the $p + {}^{207}$Tl binding potentials and spectroscopic factors were taken from the systematic reanalysis of $(d, {}^3\mathrm{He})$ data of Kramer *et al.* [15]. The exit channel $^4\mathrm{He} + {}^{207}$Tl OMP used the global parameter set of Ref. [16]. The ^{208}Pb $B(E3)$ and $B(E2)$ values, together with the corresponding nuclear deformation lengths, were as used in Ref. [7].

The bare potential was obtained by fitting the 33 MeV $^3\mathrm{H} + {}^{208}$Pb elastic scattering data of England *et al.* [17] by searching on the entrance channel OMP parameters in a calculation with all the inelastic and pickup couplings listed above included. The resulting potential parameters are: $V = 119.1$ MeV $r_0 = 1.24$ fm, $a_0 = 0.754$ fm, $W_\mathrm{D} = 19.1$ MeV, $r_\mathrm{D} = 1.20$ fm, $a_\mathrm{D} = 0.861$ fm, $V_\mathrm{so} = 2.1$ MeV, $r_\mathrm{so} = 1.11$ fm, and $a_\mathrm{so} = 0.16$ fm where the potentials have standard Woods-Saxon or Woods-Saxon derivative forms and the notation of Ref. [18] is used. The starting point for the search was potential A of Table 3 of England *et al.* [17]. Since there are no analyzing power data available, only the depth of the spin-orbit potential (V_so) was searched on in addition to the central potential components. These bare potential parameters were held fixed for all subsequent calculations.

The CC fit is presented in Fig. 1 as the solid line; the dashed line represents the angular distribution for the bare potential with inelastic and pickup couplings switched off. The generally small difference between the solid and dashed curves suggests that in this case the contribution of the couplings is not large and is similar to that seen for 33 MeV $^3\mathrm{He} + {}^{208}$Pb in Ref. [7]. However, the present data exhibit the pronounced oscillations due to nearside/farside interference whereas for 33 MeV $^3\mathrm{He} + {}^{208}$Pb there is a smooth fall-off with angle characteristic of nearside dominance. Thus, as expected, the difference in Coulomb barriers between the

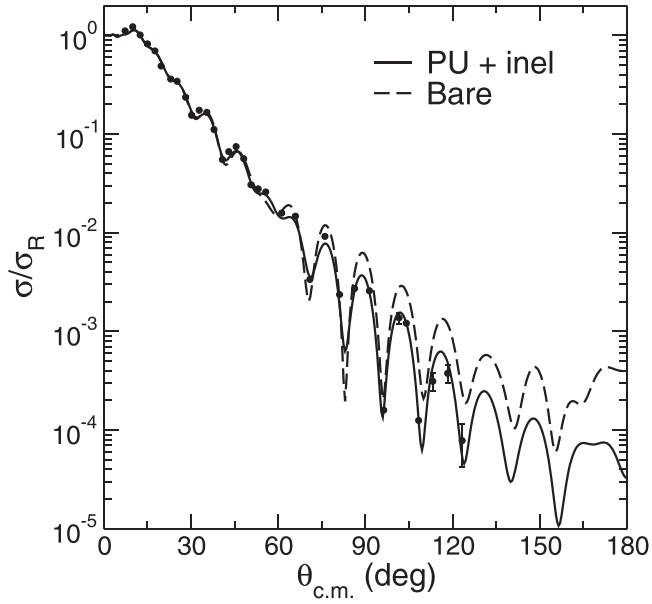

FIG. 1. For 33 MeV ^{3}H on ^{208}Pb, the solid line is the differential cross section for the full coupled channel calculation with coupling to pickup (PU) and inelastic (inel) channels with fitted optical model parameters. The dashed line represents the result of a calculation using the bare potential alone, i.e., with all couplings switched off.

two systems is important and significantly influences the scattering.

III. DETERMINING THE DPPs

The DPP due to a particular coupling or set of couplings is determined as the difference between the potential found by inversion of S_{lj} obtained from the corresponding CC calculation and the bare potential of that calculation. For example, to determine the DPP due to the combined effect of pickup and inelastic coupling, subtract the bare potential from the potential found by inverting S_{lj} when pickup and inelastic couplings are included.

To give an indication of the relative importance of the coupling influence on the OMP compared to the bare potential, Fig. 2 compares the four components of the bare potential (dashed lines) with the potential (solid lines) found by inversion that exactly reproduces S_{lj} generated by coupling to both pickup to the five states of ^{207}Tl (PU) and inelastic excitation of the two ^{208}Pb states (inel). The difference between the solid and dashed lines represents the DPP when there is both pickup and inelastic coupling.

The DPPs will be displayed below, but on the scale of Fig. 2 the attraction around 4 fm and the repulsion around 8 fm in the real central term are just perceptible. The contributions to the imaginary central term and the spin-orbit terms are relatively more conspicuous. However, replacing just the real central term of the inverted potential with the bare real central term in an optical model calculation, without modifying the other components, destroys the fit to the data from about 60° outwards, so the small real central DPP must, perhaps surprisingly, be considered to be significant.

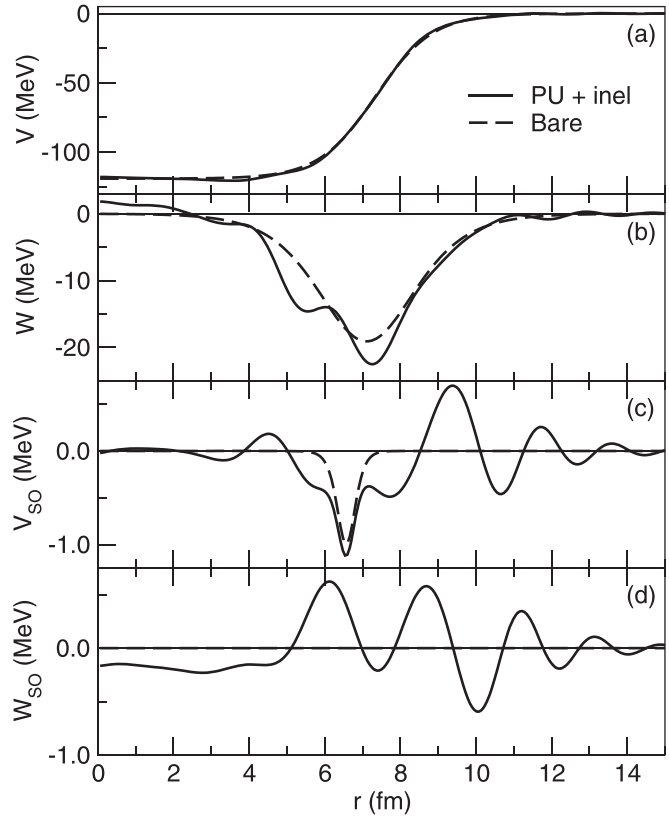

FIG. 2. For 33 MeV ^{3}H on ^{208}Pb, the bare potential (dashed lines) and the inverted potential including pickup and inelastic coupling contributions (solid lines). From the top downwards, the real central, imaginary central, real spin-orbit, and imaginary spin-orbit components.

IV. RADIAL FORMS OF THE DPPs

Figure 3 presents the four components of the DPP due to pickup only (PU) as dashed lines and those due to inelastic coupling only (inel) as dotted lines. The solid lines in Fig. 4 present the full DPP with both inelastic and pickup coupling; the dashed lines in this figure present the sum of the DPPs due to pickup alone and inelastic coupling alone. We comment later on the implications of the difference for dynamical nonlocality. The scale of Fig. 4 is very different to the scale of Fig. 2, but the attraction between about 2 and 8 fm, visible in the PU + inel real component in Fig. 4, is discernible in Fig. 2, as is the repulsion around 9 fm. The imaginary central part becomes less absorptive for $r < 2$ fm. The wavy features in various components are characteristic of l-independent potentials that are S_{lj} equivalent to l-dependent potentials. Such l-dependence is a property of the formal DPP [9–11].

V. EVALUATING THE DPPs

A. General remarks

Characteristic properties of the DPPs for different combinations of couplings are presented in the upper half of Table I in terms of the differences between corresponding properties of the inverted and bare potentials. This table employs the

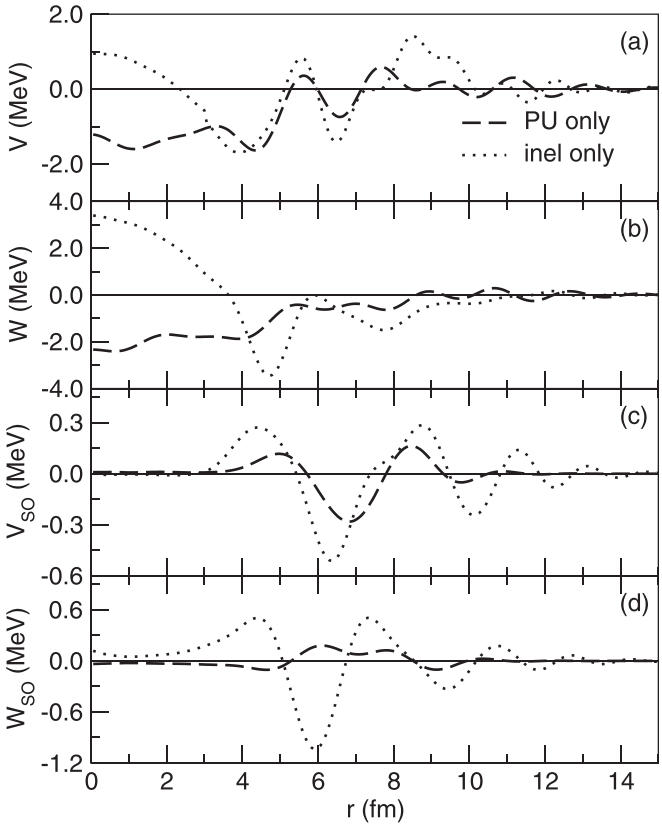

FIG. 3. For 33 MeV ^{3}H on ^{208}Pb, the dashed lines present the DPP due to the coupling to pickup channels and the dotted lines present the DPP due to coupling to the inelastic channels. The top panel (a) presents the real central DPP, (b) presents the imaginary central DPP, (c) presents the real spin-orbit DPP, and (d) presents the imaginary spin-orbit DPP.

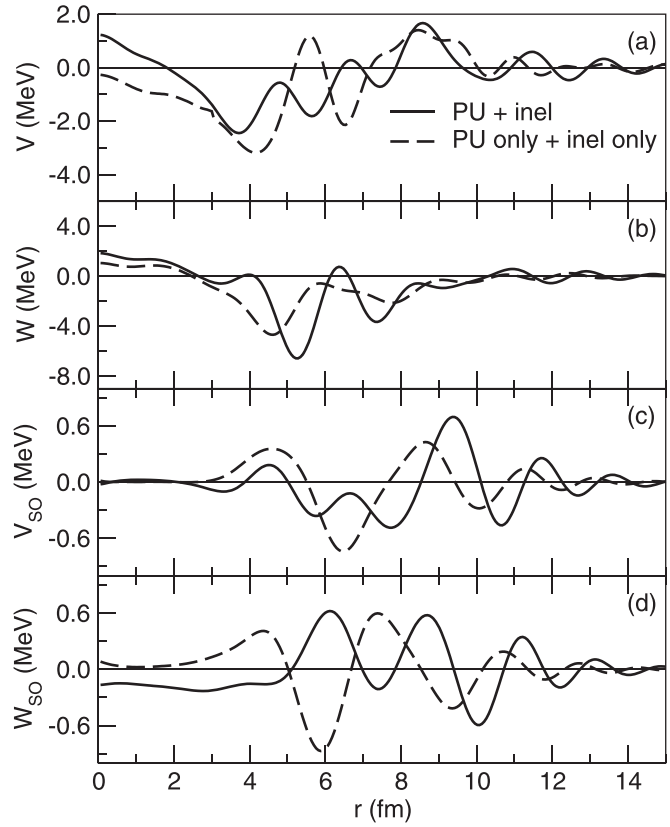

FIG. 4. For 33 MeV ^{3}H on ^{208}Pb, the solid lines present the DPP due to coupling to both pickup and inelastic channels. The dashed lines present the sum of the DPPs to just the pickup channels and to just the inelastic channels. From the top downwards, the real central, imaginary central, real spin-orbit and imaginary spin-orbit components of the respective DPPs.

standard normalization of Ref. [9] for $J_{\rm R}$ and $J_{\rm IM}$, the volume integrals of the real and imaginary potentials, and $\Delta J_{\rm R}$, for example, denotes the volume integral of the real central component of the DPP due to the indicated coupling. We use the standard sign convention for $J_{\rm R}$ and $J_{\rm IM}$ in which a positive sign represents attraction or absorption. Thus, a negative $\Delta J_{\rm R}$ represents a net repulsive contribution from the specified coupling. However, figures showing potentials use natural signs: negative for attraction or absorption. Unsurprisingly, $\Delta J_{\rm IM}$, the change in the volume integral of the imaginary central term due to coupling, is positive in all cases indicating added absorption, as expected.

For each coupling, Table I also presents Δ(CS), the change in reaction cross section due to the coupling. The quantity R is the ratio of Δ(CS) to $\Delta J_{\rm IM}$, the change, due to coupling, in the volume integral of the imaginary central potential

$$R = \frac{\Delta(\mathrm{CS})}{\Delta J_{\rm IM}}. \qquad (1)$$

R varies over a much smaller range than Δ(CS) or $\Delta J_{\rm IM}$ separately.

Table I additionally presents the 'State CS' which is the total (^{3}H, ^{4}He) and/or (^{3}H, ^{3}H$'$) cross section in mb to the pickup states and/or the collective states as specified in the text. The State CS gives a measure of the coupling and is generally not equal to the change in reaction cross section Δ(CS). The relationship between these two quantities varies widely for different couplings. Various regularities emerged for ^{3}He and ^{3}H on ^{16}O and ^{40}Ca targets and for ^{3}He on ^{208}Pb; to facilitate comparisons, we present values of $R_{\rm CS}$ defined as the ratio of Δ(CS) to State CS.

Regarding the comparison of the DPPs for different couplings, for a given projectile (^{3}H or ^{3}He) all calculations were carried out with a fixed bare potential. There are both expected and unexpected results in Table I:

(1) For pickup coupling Δ(CS) and State CS are equal, see line 1. Although at first sight plausible, it is in fact unusual over a wide range of similar cases.
(2) Although State CS is larger for inelastic coupling (line 2) than for pickup (line 1), inelastic coupling actually leads to a negative Δ(CS). Inelastic coupling of substantial cross section has *reduced* the total cross section, hence the negative $R_{\rm CS}$.
(3) Very unusually, $\Delta J_{\rm R}$ is positive for PU coupling, although very small. In all other cases known to us, pickup coupling generates net repulsion. An example is in line 1a, where we see that for PU coupling of ^{3}He on ^{208}Pb, $\Delta J_{\rm R}$ is negative [7].

TABLE I. In lines 1 to 4, for ^{3}H scattering from ^{208}Pb at 33 MeV, volume integrals ΔJ (in MeV fm^3) of the four components of the DPP induced by (^{3}H, ^{4}He) pickup coupling ('PU') and/or coupling to inelastic states ('inel'). The coupled states for ^{208}Pb are given in Sec. II; the excitation energies of the states, in MeV, are all specified. The $\Delta R_{\rm rms}$ column gives the change in rms radius of the real central component (in fm). The final four columns present the change in the total reaction cross section induced by the coupling, the calculated cross section to the specific coupled channels, the ratio R and the ratio $R_{\rm CS}$, both defined in the text. Note that in line 1 positive $\Delta J_{\rm R}$ corresponds to a small net attraction, an anomaly since PU is generally repulsive. The quantities Δ(CS) and State CS are given in mb. Line 4 presents arithmetic sums of the quantities in line 1 and line 2. Lines 1a to 4a present corresponding values for the case of ^{3}He on ^{208}Pb at the same energy [7].

L	Reaction	$\Delta J_{\rm R}$	$\Delta J_{\rm IM}$	$\Delta J_{\rm RSO}$	$\Delta J_{\rm IMSO}$	$\Delta R_{\rm rms}$	Δ(CS)	State CS	R	$R_{\rm CS}$
1	PU	0.81	2.806	0.105	−0.138	−0.0111	1.9	1.90	0.68	1.0
2	Inel	−1.35	5.75	0.126	0.294	−0.0269	−2.0	4.72	−0.35	−0.42
3	Inel and PU	0.33	9.436	0.187	−0.454	−0.023	−1.3	6.51	−0.14	−0.20
4	Sum of Inel, PU	−0.54	8.556	0.231	0.157	−0.038	−0.1	6.62	−0.02	−0.015
1a	PU ^{3}He	−2.33	6.286	0.520	−0.089	−0.603	−16.4	2.91	−2.6	−5.63
2a	Inel ^{3}He	−0.52	1.995	0.310	−1.088	−0.434	−1.4	4.90	−0.70	−0.29
3a	Inel and PU, ^{3}He	−1.68	8.889	0.690	−0.869	−0.063	−18.0	7.88	−2.02	−2.28
4a	Sum of Inel, PU, ^{3}He	−2.85	8.281	0.812	−1.177	−1.037	−17.8	7.81	−2.15	−2.28

(4) In line 4 the sums of the inelastic and pickup contributions to the volume integrals are not equal to the values in line 3 when inelastic coupling and pickup are both included. This is evidence of the dynamical nonlocality of the DPPs generated by the coupling, see Ref. [12] and references therein.

(5) Δ(CS) does not depend upon the inversion of S_{lj}, so the disparity between the 'Inel and PU' and 'Sum of Inel, PU' values of Δ(CS) is not a consequence of non-additivity of local DPPs. It does, however, indicate an interaction between channels that are not directly coupled.

(6) In the same way, the evident nonadditivity of the State CS quantities is also independent of inversion.

(7) Inelastic and pickup coupling generate a negative change in the rms radius of the real potential, consistent with effects for ^{3}He and ^{3}H scattering on lighter nuclei [7,8], although significantly smaller in magnitude.

Comment on points 1 and 2: Other cases in which the change in total cross section is less than the state cross section, $R_{\rm CS} < 1$, or even negative, may be found in Refs. [7,8]. There are cases for light targets where $R_{\rm CS} > 1$, in which case the reaction appears to act as a doorway to further processes. However, an 'anti-doorway' effect as in all cases in Table I, except PU for ^{3}H, is most common.

B. Comparison with the ^{3}He case

Lines 1a to 4a of Table I present data from Ref. [7] and enable a comparison with the corresponding results for ^{3}He on ^{208}Pb. Here we note specific differences between the two cases which are seen more explicitly in Figs. 5 and 6.

(1) Unlike the ^{3}H case, for ^{3}He the real DPP for pickup is overall repulsive, in accord with all pickup cases known to us, and much stronger in magnitude than for ^{3}H, in agreement with expectations due to the pickup strength.

(2) For pickup coupling with ^{3}He on ^{208}Pb the State CS is greater than for ^{3}H, as expected. Not expected is the large magnitude but negative Δ(CS) and hence negative $R_{\rm CS}$. Why does pickup coupling substantially

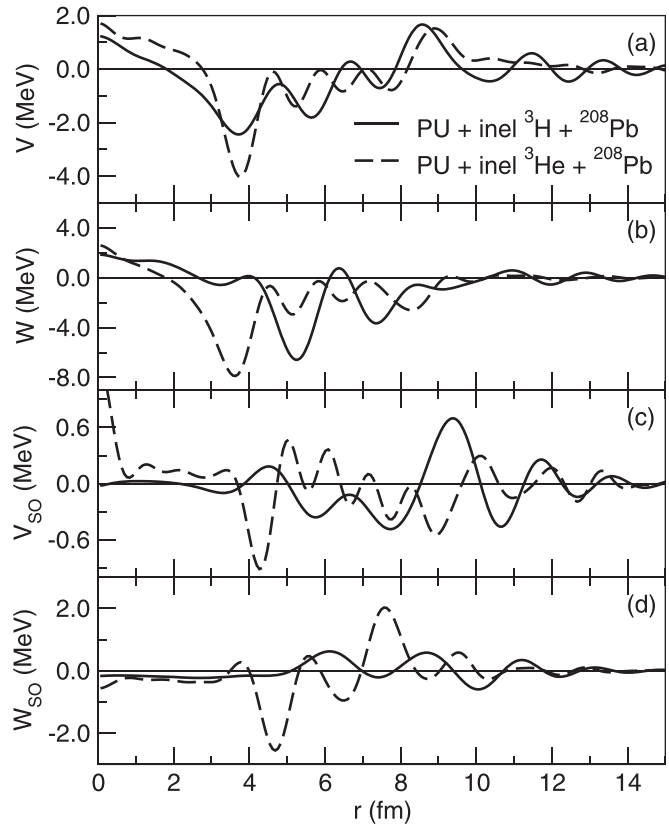

FIG. 5. A direct comparison of the DPPs for 33 MeV ^{3}H and ^{3}He on ^{208}Pb when pickup and inelastic coupling are both included. The solid lines present the DPP for ^{3}H and the dashed lines are for ^{3}He. In each case the lines present the DPPs when pickup channels and inelastic coupling are both included. From the top downwards, the real central, imaginary central, real spin-orbit and imaginary spin-orbit components of the respective DPPs.

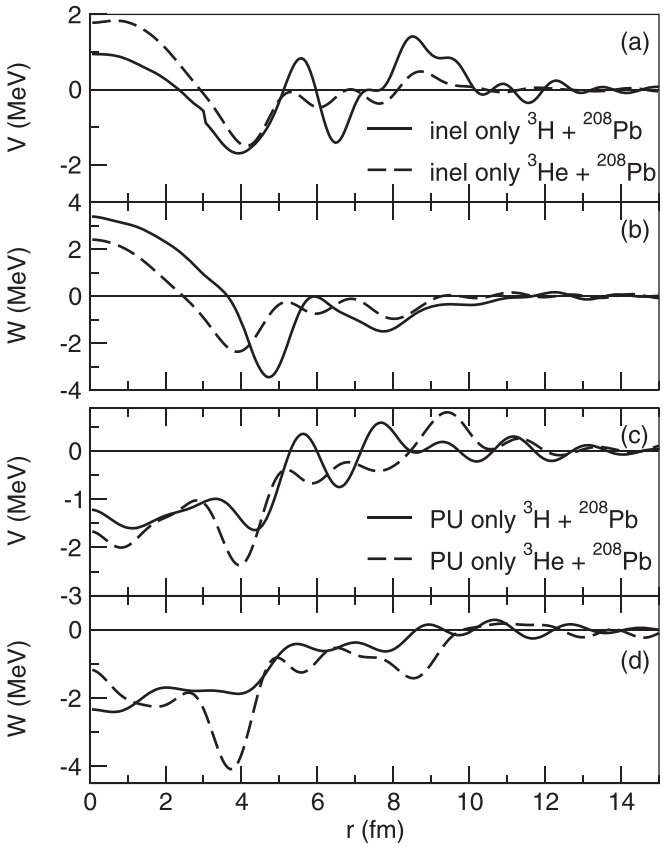

FIG. 6. For 33 MeV ^{3}H and ^{3}He on ^{208}Pb, a direct comparison of the DPPs for both pickup and inelastic coupling. (a) and (b) compare the DPPs due to inelastic coupling only for ^{3}H (solid lines) and ^{3}He (dashed lines) with the real parts in (a) and the imaginary parts in (b). (c) and (d) compare the DPPs due to pickup coupling only for ^{3}H (solid lines) and ^{3}He (dashed lines) with the real parts in (a) and the imaginary parts in (b). The spin-orbit terms are not compared in this figure.

reduce the ^{3}He reaction cross section? For ^{3}H, Δ(CS) is equal to State CS, the zeroth order guess for this relationship.

(3) Comparing lines 3a and 4a with lines 3 and 4 we note a very similar pattern of nonadditivity of volume integrals, a consistent effect of dynamical nonlocality.

(4) The significantly larger value of $\Delta J_{\rm IM}$ in line 1a of Table I, compared to the corresponding value in line 1, is linked to the much deeper dip in W around 3.8 fm for the ^{3}He PU case compared to the ^{3}H PU case, see panel (d) of Fig. 6.

Figure 5 exhibits many similarities between the total (PU + inel) DPPs for 33 MeV ^{3}H and ^{3}He on ^{208}Pb. Leaving to one side the spin-orbit components of the DPPs which are more difficult to interpret due to the undularities in the ^{3}He + ^{208}Pb case in particular, it is striking just how similar the total (PU + inel) DPPs are for the two systems, cf. Fig. 5(a) and (b). This is especially so for the real central DPPs; for the imaginary central terms the main absorptive dip for ^{3}H + ^{208}Pb appears shifted to larger radii compared to ^{3}He + ^{208}Pb by about 1.5 fm but the shapes are qualitatively similar for the two projectiles.

Figure 6 provides more detail, presenting the central terms of the inel only and PU only DPPs. For example, the inel only DPPs, Fig. 6(a) and 6(b), show similar behavior for r less than about 4 fm, V tending to be repulsive and W tending to be emissive at the nuclear center. This is unlikely to be detectible in elastic scattering because the projectiles would be strongly absorbed in this radial region, although notch tests show some sensitivity to the real central potential even at a radius of 2 fm. The apparent undularity of the DPP can be associated with the representation of an l-dependent potential by an l-independent potential. A recent work explicitly relating undularity to underlying l dependence is Ref. [19]. The shift in the main absorptive dip of the ^{3}H total (PU + inel) imaginary DPP is largely due to the inelastic (inel) coupling, see Fig. 5(b). The negative imaginary term from 5 fm outwards for the ^{3}H inel case in Fig. 6(b) reflects the $\Delta J_{\rm IM} = 5.75$ in line 2 of Table I, which is much larger than the value for ^{3}He in line 2a of that table.

The real terms also exhibit a general similarity of form for the ^{3}H and ^{3}He cases. Nevertheless, there are some apparently significant differences. For example, the positive bump around 9.5 fm in the real potential for the ^{3}He PU only case probably accounts for the -2.33 $\Delta J_{\rm R}$ in line 1a of Table I. The r^2 weighting of the volume integral could explain why the similar bump at about 7.5 fm in the ^{3}H PU only real DPP is not sufficient to give an overall repulsive $\Delta J_{\rm R}$ in this case, see Fig. 6(c) and line 1 of Table I.

C. Coulomb excitation

The contribution of Coulomb excitation to inelastic scattering of ^{3}He and ^{3}H on ^{208}Pb is not large. Nevertheless, the differences and also similarities between the contributions to ^{3}H and ^{3}He inelastic scattering are of interest. The real and imaginary central DPPs for inelastic scattering are compared in Fig. 7, both with and without Coulomb excitation, denoted Coulex in the figure. Note that the V panels have different vertical scales from the W panels.

In Fig. 7, the ^{3}He and ^{3}H DPPs exhibit various similar features, both with Coulomb excitation (dashed lines) and without (solid lines). For the ^{3}He case the Coulomb excitation generally reduces the magnitude of the both the real and imaginary terms, except where there is evidence for the interference of amplitudes. One effect is to dampen the undularities and, in particular, reduce the dips around 4 fm which represent local maxima of attraction and absorption. For the ^{3}H case, forward of 4 fm, inelastic Coulomb coupling has a similar but attenuated effect as for ^{3}He. It also modifies the repulsive region near 9 fm. The Coulomb excitation has damped down the undularity in the real component between 5 fm and 10 fm. For ^{3}H, the dip in the imaginary term around 5 fm, like the similar dip for ^{3}He at a slightly smaller radius, is reduced by the inclusion of Coulomb excitation. For ^{3}H in particular, Coulomb excitation has little effect for $r < 3$ fm. The double charge on ^{3}He has not conspicuously doubled the effect of the Coulomb excitation, except perhaps for the real term near the origin.

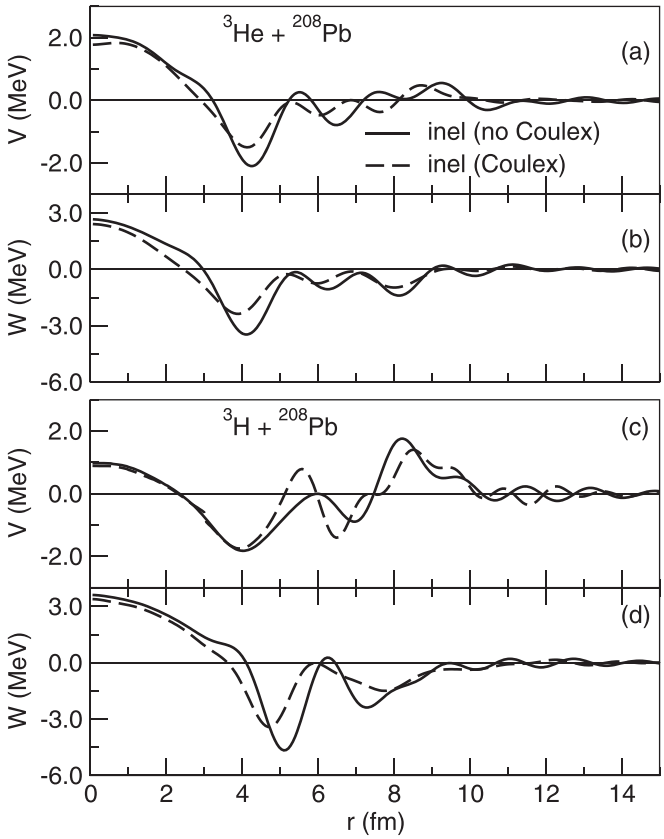

FIG. 7. Direct comparison of the DPPs for inel only coupling with (dashed lines) and without (solid lines) Coulomb excitation for 33 MeV ^{3}He + ^{208}Pb (a) and (b) and 33 MeV ^{3}H + ^{208}Pb (c) and (d) elastic scattering. The spin-orbit terms are not compared in this figure.

VI. SUMMARY AND COMPARISON WITH PREVIOUS WORK

The present work completes a comparison of coupling contributions to the interaction of mass three projectiles at about 30 MeV with ^{16}O, ^{40}Ca, and ^{208}Pb. Aspects of the interaction of mass three nuclei with the lighter targets may be found in two previous works: Ref. [7] presents the contributions of pickup and inelastic coupling to the scattering of ^{3}He on ^{16}O, ^{40}Ca, and ^{208}Pb, and Ref. [8] presents pickup and inelastic coupling contributions to the scattering of ^{3}H on ^{16}O and ^{40}Ca. In this work we concentrate on the comparison of ^{3}He and ^{3}H interactions with ^{208}Pb, see the last four lines of Table I.

For ^{3}He on ^{208}Pb, ΔJ_R is negative for PU, the usual overall repulsion for pickup coupling. There is also overall repulsion for ^{3}He inelastic coupling but the effect is smaller in magnitude. The situation is quite different for ^{3}H scattering: for pickup coupling ΔJ_R is positive though small, indicating overall attraction. For ^{3}H, inelastic coupling generates absorption, as expected, although rather surprisingly substantially more than for ^{3}He. ΔJ_{IM} is nearly three times what it is for ^{3}He. Clearly, the increased importance of Coulomb excitation for ^{3}He does not lead to more absorption from the elastic channel.

For ^{3}H, the change in the reaction cross section, Δ(CS), for inelastic coupling is much less than the cross section (State CS) to the excited states involved and is actually negative. The phenomenon of reaction channels *reducing* the total cross section, CS, is not unique to the present case, and can be seen for ^{3}He too, for both pickup and inelastic coupling.

Reference [8] does not report coupling effects for ^{3}H on ^{208}Pb but, with Ref. [7] allows a comparison of coupling effects of ^{3}He and ^{3}H on ^{40}Ca. The DPPs for ^{40}Ca follow the same general pattern for ^{3}He and ^{3}H but they are greater in magnitude for ^{3}He than for ^{3}H. For ^{3}He and ^{3}H on ^{208}Pb a similar situation occurs for the pickup coupling, but for the inelastic coupling the reverse is true, i.e., the ^{3}H inel DPPs are significantly greater in magnitude than those for ^{3}He. It is not obvious why this should be so, for two reasons. First, the orbitals involved in the pickup process are notably different for ^{3}H and ^{3}He on ^{208}Pb, unlike the lighter targets which are self-conjugate. Second, the much greater charge of the ^{208}Pb target means that the difference in Coulomb barriers between ^{3}H and ^{3}He is much more marked; the ^{3}He on ^{208}Pb data are in the nearside dominated scattering regime whereas the ^{3}H on ^{208}Pb data show the characteristic oscillations associated with nearside/farside interference. One might *a priori* have expected the inelastic coupling to give rise to a stronger DPP for ^{3}He on the basis of the increased Coulomb excitation, but this is obviously not the case; the difference in Coulomb barriers would seem to be playing an important role here, via the difference in scattering regimes of the two systems. One line of future research could involve an investigation of the evolution as a function of bombarding energy of the DPPs for the ^{3}He and ^{3}H + ^{208}Pb systems, which could give some insight into this question.

Finally, perhaps the most striking conclusion of this work, together with Refs. [7] and [8], is not the differences between the ^{3}H and ^{3}He DPPs for a given target but how similar they are, even for the ^{208}Pb target. This may go some way to explain the observation that the global ^{3}He OMP of Pang *et al.* [20] works equally well for ^{3}H elastic scattering with just a simple Coulomb correction term to the depths of the real and imaginary central parts. Although the present results are suggestive, a full answer to this question requires extensive further work involving a wider range of targets and an investigation of the energy dependence of the DPPs.

We have applied currently standard calculational methods for direct reactions. As nuclear theory undergoes developments involving new theoretical and computational methods, the present work suggests that a future comprehensive account of ^{3}H or ^{3}He scattering should include, among other things, outgoing ^{4}He.

[1] M. Kohno, Phys. Rev. C **98**, 054617 (2018).
[2] H. F. Arellano and G. Blanchon, Phys. Rev. C **98**, 054616 (2018).
[3] M. Vorabbi, M. Gennari, P. Finelli, C. Giusti, P. Navrátil, and R. Machleidt, Phys. Rev. C **103**, 024604 (2021).

[4] H. F. Arellano and G. Blanchon, Eur. Phys. J. A **58**, 119 (2022).
[5] Z. Zhang, R. R. Xu, Z. Y. Ma, Z. G. Ge, Y. Tian, D. Y. Pang, X. D. Sun, Y. L. Jin, X. Tao, Y. Zhang, and J. M. Wang, Nucl. Phys. A **990**, 1 (2019).
[6] R. S. Mackintosh and N. Keeley, Phys. Rev. C **81**, 034612 (2010).
[7] R. S. Mackintosh and N. Keeley, Phys. Rev. C **100**, 064613 (2019).
[8] N. Keeley and R. S. Mackintosh, Phys. Rev. C **102**, 064611 (2020).
[9] G. R. Satchler, *Direct Nuclear Reactions* (Clarendon Press, Oxford, 1983).
[10] H. Feshbach, Ann. Phys. (NY) **5**, 357 (1958); **19**, 287 (1962).
[11] G. H. Rawitscher, Nucl. Phys. A **475**, 519 (1987).
[12] N. Keeley and R. S. Mackintosh, Phys. Rev. C **90**, 044602 (2014).
[13] I. J. Thompson, Comput. Phys. Rep. **7**, 167 (1988).
[14] I. Brida, S. C. Pieper, and R. B. Wiringa, Phys. Rev. C **84**, 024319 (2011).
[15] G. J. Kramer, H. P. Blok, and L. Lapikás, Nucl. Phys. A **679**, 267 (2001).
[16] V. Avrigeanu, M. Avrigeanu, and C. Mănăilescu, Phys. Rev. C **90**, 044612 (2014).
[17] J. B. A. England *et al.*, Nucl. Phys. A **475**, 422 (1987).
[18] C. M. Perey and F. G. Perey, At. Data Nucl. Data Tables **17**, 1 (1976).
[19] R. S. Mackintosh, Phys. Rev. C **94**, 034602 (2016).
[20] D. Y. Pang, P. Roussel-Chomaz, H. Savajols, R. L. Varner, and R. Wolski, Phys. Rev. C **79**, 024615 (2009).